ORIGINAL PAPER

Structures and optical properties of zinc oxide nanoclusters: a combined experimental and theoretical approach

Cahit Orek[1,2] · Serhat Keser[3] · Omer Kaygili[1] · Piotr Zuchowski[4] · Niyazi Bulut[1]

Abstract

Context In this study, theoretical and experimental analysis of the electrical, optical, and structural properties of a wurtzite-like zinc oxide (ZnO) nanostructure has been done. To investigate how quantum confinement affects the optical characteristics, two distinct ZnO clusters in nanowire structures have been investigated. The $[(ZnO)_{55}(H_2O)_4]$ system's HOMO–LUMO band gap (BG) was calculated to be 2.99 eV, which is quite close to the experimental measurement. It was found that the BG decreases with the increase in the number of atoms in the cluster in connection with the quantum confinement in nanoclusters. In addition, the lowest excitation energy in TD-DFT calculations of the identical system is in fairly good agreement with the experimental value with a difference of 0.1 eV. We conclude that the CAM-B3LYP functional has highly successful in reproducing the experimental data reported in the present study and previously reported experimental data.

Methods The geometrical optimization of two different sizes of ZnO clusters ($[(ZnO)25(H2O)4]$ and $[ZnO)55(H2O)4]$) was performed using the CAM-B3LYP functional with no symmetry constraints applied in the gas phase. LANL2DZ basis sets were used for the Zinc (Zn) atom and 6-31G* basis sets for the O and H atoms. To determine their optical and electronic properties, excited state calculations of the pre-optimized structures were performed using the Time-Dependent DFT (TD-DFT) method. Multiwfn, Gaussum 3.0, and GaussView 5.0 programs were used to visualize the results.

Keywords Zinc oxide · TD-DFT · Quantum confinement · Energy band gap · Density of states

Introduction

ZnO is a semiconductor material having chemical and thermal stability and is excellent for short-wavelength optoelectronic applications due to its high exciton binding energy of 60 meV and direct band gap of 3.37 eV at ambient temperature. The high exciton binding energy of this compound gives it UV luminescence and efficient excitonic emission properties [1].

In addition, non-toxicity, good permeability and electrical conductivity, high electron mobility and low cost make ZnO one step ahead of other metal oxides [2]. Thanks to these properties, ZnO nanomaterials are suitable for producing advanced technology devices such as solar cells, photocatalysts, sensors, detectors and light-emitting diodes [3–7]. When analyzed morphologically, it is seen that ZnO materials can be in rod, wire, flower, leaf, arch and tube structures. Morphological properties, crystal structure and size of ZnO materials affect their electrical and optical properties [8–13].

ZnO semiconductor is a compound formed by the combination of sp^3 covalent and ionic bonding of Zn and O atoms in group II-VI of the periodic table. ZnO can be found in wurtzite, zinc blende and rocksalt crystal structures and its density is 5.606 g/cm^3. The wurtzite is the thermodynamically stable phase at room temperature, with hexagonal unit cells.

One Zn atom coordinates with four O atoms in the crystal structure to form a tetrahedral arrangement. This result in a crystal structure without a center of symmetry and ZnO has two polar surfaces facing each other, each ending with

✉ Cahit Orek
  cahitorek@gmail.com

1   Department of Physics, Faculty of Science, Firat University, 23119 Elazig, Turkey

2   Kastamonu Univ, Res & Applicat Ctr, TR-37150 Kastamonu, Turkey

3   Department of Chemical Technology, EOSB Higher Vocational School, Firat University, 23119 Elazig, Turkey

4   Institute of Physics, Faculty of Physics, Astronomy and Informatics, Nicolaus Copernicus University, Grudziadzka 5, 87-100 Torun, Poland

a single type of ion. The lack of symmetry in the crystal structure gives ZnO strong piezoelectric and pyroelectric properties and great electromechanical properties [14–17]. When the studies related to ZnO are examined [18], it found that the bandgap energies of ZnO and indium-doped ZnO samples synthesized by hydrothermal method decreased and that indium doping further increased this decrease and that the dopant concentration also decreased the photocurrent intensity. In another study [19], it was investigated the antibacterial and biocompatibility properties of synthesized ZnO and Ca-doped ZnO samples, and it was suggested that these materials have high aforementioned properties. Giannoudakos et al. [20] calculated the catalytic and adsorption properties of the un-doped, Au- and Pd-doped ZnO thin films using PC programs written in Fortran. In a similar study, El Mragui et al. [21] determined the photocatalytic and physicochemical properties of ZnO/TiO$_2$ nanomaterials. Li et al. [22] showed that the visible emission of ZnO nanomils and ZnO@ZnS micromil composites can be tuned, which may have potential applications in luminescence, electronics and sensors. Fujinami et al. [23] evaluated the adsorption and binding mechanism between Zn$_2$O$_2$ cluster and crystalline polyimide substrate by semi-experimental molecular orbital calculations and concluded that reactions involving a chemical bond between a cluster of Zn atoms and a carbonyl O atom in the polyimide take place and that the adsorption processes are almost a thermal.

Kaygili et al. [24] experimentally synthesized, characterized and theoretically modeled (DFT) ZnO powders and compared the results with each other and with the results of other studies in the literature. As a result, they found that the electron excitation of ZnO is most likely to occur at the Γ-Γ point, where the energy gap between the valence and conduction bands has the lowest value. Sheela et al. [25] tried to determine the structural, morphological, optical and photocatalytic properties of the un-doped, Ni- and Co-doped ZnO samples produced by hydrothermal method. In their review article [26], suggested that ZnO-based polymer nanocomposites have dielectric, thermal, antibacterial, biomedical, catalytic and mechanical properties and that ZnO doping of these nanocomposites improves their thermal, electrical, piezoelectric, mechanical, electromagnetic, energy storage properties and environmental application potential. Baranov et al. [27] found a decrease in the melting temperature of ZnO samples produced under high pressure and they observed a single crystal growth occurred in these samples.

Raha and Ahmaruzzaman [28] suggested that ZnO nanoparticles can be used in the treatment of diabetes by lowering blood sugar and increasing insulin levels, as well as for anticancer and antibacterial purposes by causing high inhibition on cancerous cells and bacteria, and that ZnO nanoparticles are recognized as safe substances by the FDA. Chu et al. [29] investigated the use of ZnO samples with different forms (e.g., nanoparticles, nanowires, nanoneedles, nanorods and microtubes, etc.) as UV photodetectors and they exhibited different photoelectric properties such as response, on/off ratio and response time. Puspasari et al. [30] claimed that ZnO-based antibacterial coatings have great potential in biomedical and medical fields and have shown positive results in clinical applications.

Many DFT studies have been reported in the literature on the optical, electronic and structural parameters of wurtzite-like ZnX (X = O, Se, Te and S) systems [31–34]. In these studies, Local density approximation (LDA) and generalized gradient approximation (GGA) functionalism are generally used to determine the structural parameters. However, since these functional are insufficient for determining optical and electronic properties [35–38], the B3LYP hybrid functional is used to calculate optical and electronic properties such as UV–VIS, DOS and band gap.

Here, unlike the existing studies, since the deficiencies of B3LYP functional are known, further studies using more adequate functionals are needed. To this end, the structural, optical and electronic properties of wurtzite ZnO have been calculated using the CAM-B3LYP functional. CAM-B3LYP is an exchange–correlation functional [39], which is a combination of the hybrid properties of B3LYP and long-range correction. These functional gives results very close to experimental findings, especially for UV–VIS, DOS, PL and band gap calculations where long-range interactions are important [40–42].

Materials and methods

Synthesis and characterization of ZnO sample

The synthesis procedure of the ZnO sample is given as follows: 100 mL of 40 mmol of zinc acetate dihydrate (Sigma-Aldrich) solution was prepared by using ethanol (Sigma-Aldrich) as the solvent. This solution was stirred at room temperature for 1 h, and put in an oven at 50 °C for 10 days to dry. The as-obtained powder was heated in an electric furnace at 650 °C for 1.5 h.

A Rigaku RadB-DMAX II model diffractometer utilizing CuKα radiation was used to collect the X-ray diffraction (XRD) data. A LEO EVO 40xVP model scanning electron microscope (SEM) was used to investigate the morphology of the as-produced sample.

Computational details

Owing to the effects of quantum confinement in nanostructures, the optical properties (absorption and emission) are dependent on the structural size and an energetic upward shift in the onset of absorption and emission spectra is

observed with decreasing structural size [43–45]. However, studies on ZnO nano-structures have shown that the main directions responsible for quantum confinement effects are the crystal axes [0001] and [1010] [46]. For this reason, in the present study, 2D ZnO cluster geometries of different sizes were formed starting from the bulk wurtzite structure to make a convenient comparison with the experimental data.

Similarly, in the past studies on Zn-based II-VI semiconductor nano-structures [47–49], an unrealistically high dipole moment in the c direction due to Zn- and O-terminated (0001) and (000) surfaces in non-centrosymmetric WZ structures is observed and this dipole moment makes the structure unstable [47, 48]. For this reason, in accordance with the literature [47, 50, 51], polar surfaces were saturated with dissociating water molecules. Zinc atoms on polar surfaces were saturated with OH^- and oxygen atoms were saturated with H^+ ions. Considering that protic solvents are used in the synthesis of semiconductor nanostructures, it should be emphasized that this saturation process is not just a calculation trick.

The geometrical optimization of ZnO clusters of two different sizes ($[(ZnO)_{25}(H_2O)_4]$ and $[ZnO)_{55}(H_2O)_4]$) was performed using the CAM-B3LYP [39] functional as implemented in the GAUSSIAN 09 suite of programs [52] and Gaussian type orbits (GTO) basis sets. For simplicity, the calculations were performed in the gas phase and no symmetry constraints were applied. In the calculations, LANL2DZ (Los Alamos National Lab 2 Double Zeta) [53] for Zinc (Zn) atom and 6-31G* basis sets for O and H atoms were used. In addition, to determine the optical (UV) and electronic (band gap) properties of ZnO clusters, excited state calculations of the pre-optimized structures were performed in the gas phase by Time-Dependent DFT (TD-DFT) [54] method. Multiwfn [55], Gaussum 3.0 [56] and GaussView 5.0 [57] programs were used to visualize the data obtained from the calculations.

Findings and discussion

The XRD plot of the sample confirms the polycrystalline ZnO structure with the hexagonal crystal structure (JCPDS PDF No: 36–1451) (Fig. 1). No impurity phase was detected. Table 1 lists the observed and estimated values of the distance between two adjacent planes (d) and 2θ angles for each Miller index (hkl). Both the calculated and the observed values are in agreement.

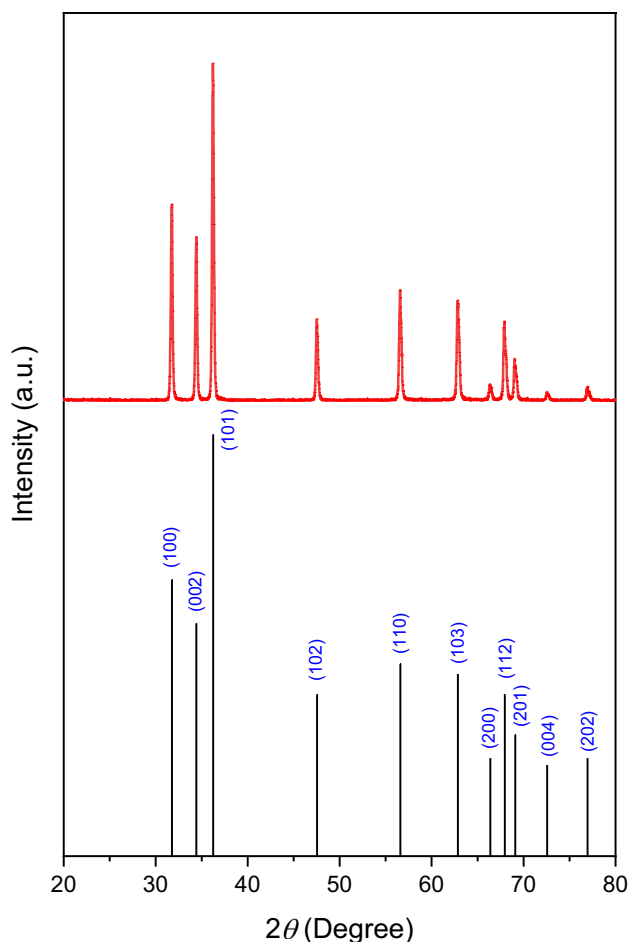To calculate the crystallinity percent ($X_C\%$) of ZnO, the following relation was used [58]

Fig. 1 XRD pattern of the ZnO sample

$$X_C\% = \frac{\sum A_C}{\sum A_C + \sum A_A} \times 100 \qquad (1)$$

where ΣA_C and ΣA_A are the total areas under crystal and amorphous peaks, respectively. This value was estimated to be 95.7% in the present study.

The lattice parameters (a and c) and unit cell volume (V) were found to be $a = 0.3251$ nm, $c = 0.5207$ nm, and $V = 0.0477$ nm.^{3} by using Eqs. (2) and (3), respectively [59]

$$\frac{1}{d^2} = \frac{4}{3}\left(\frac{h^2 + hk + k^2}{a^2}\right) + \frac{l^2}{c^2} \qquad (2)$$

$$V = 0.866a^2c \qquad (3)$$

Both Scherrer and Williamson-Hall equations were used to calculate the crystallite size, respectively [24]

$$D_S = \frac{0.9\lambda}{\beta\cos\theta} \qquad (4)$$

Table 1 The comparison of the observed and calculated values of the d and 2θ for the as-produced ZnO

h	k	l	d_{obs} (nm)	d_{col} (nm)	Δd (n)m	$2\theta_{obs}$ (°)	$2\theta_{al}$ (°)	$\Delta\theta$ (°)
1	0	0	0.281684	0.281565	0.00119	31.740	31.754	−0.014
0	0	2	0.260340	0.260367	−0.00027	34.420	34.416	0.004
1	0	1	0.247145	0.247677	−0.00532	36.320	36.239	0.081
1	0	2	0.191181	0.191162	0.00018	47.520	47.525	−0.005
1	1	0	0.162582	0.162562	0.00020	56.560	56.568	−0.008
1	0	3	0.147759	0.147757	0.00002	62.840	62.841	−0.001
2	0	0	0.140824	0.140782	0.00042	66.320	66.342	−0.022
1	1	2	0.137927	0.137892	0.00035	67.900	67.920	0.020
2	0	1	0.135960	0.135903	0.00056	69.020	69.053	0.033
0	0	4	0.130205	0.130183	0.00021	72.540	72.554	0.014
2	0	2	0.123764	0.123839	−0.00075	76.980	76.925	0.055

$$\beta\cos\theta = \frac{0.9\lambda}{D_{WH}} + 4\varepsilon\sin\theta \tag{5}$$

where β, λ and ε are the full width at half maximum, wavelength, and lattice strain, respectively. The D_S value was found to be 32.51 nm, and the D_{WH} and ε values estimated from the $\beta\cos\theta$ vs. $4\sin\theta$ graph shown in Fig. 2a were calculated to be 46.84 nm and 1.02×10^{-3}, respectively. To calculate the stress (σ), the Eq. (6) was used:

$$\beta\cos\theta = \frac{0.9\lambda}{D_{WH}}\frac{4\sigma\sin\theta}{Y} \tag{6}$$

To estimate Young's modulus (Y), the following relation was used

$$Y = \frac{\left[h^2 + \frac{(h+2k)^2}{3} + \left(\frac{al}{c}\right)^2\right]^2 \times 10^{12}}{7.858\times\left(h^2+\frac{(h+2k)^2}{3}\right)^2 + 6.940\times\left(\frac{al}{c}\right)^4 + 19.158\times\left(h^2+\frac{(h+2k)^2}{3}\right)\left(\frac{al}{c}\right)^2} \tag{7}$$

The slope of the $\beta\cos\theta$ vs. $4\sin\theta/Y$ graph (Fig. 2b) gives the σ value. This value was computed to be 88.56 MPa.

To calculate the energy density (u), the following relation was used:

$$\beta\cos\theta = \frac{0.9\lambda}{D_{WH}} + 4\sin\theta\left(\frac{2u}{Y}\right)^{1/2} \tag{8}$$

The u value was calculated from the $\beta\cos\theta$ vs. $2^{5/2}\sin\theta\, Y^{-1/2}$ graph (Fig. 2c), and this value was found to be 52.90 kJ m^{-3} in the present work.

The bond length (L) between Zn and O, and atomic packing factor (APF) were calculated by using Eqs. (9) and (10), respectively [60]
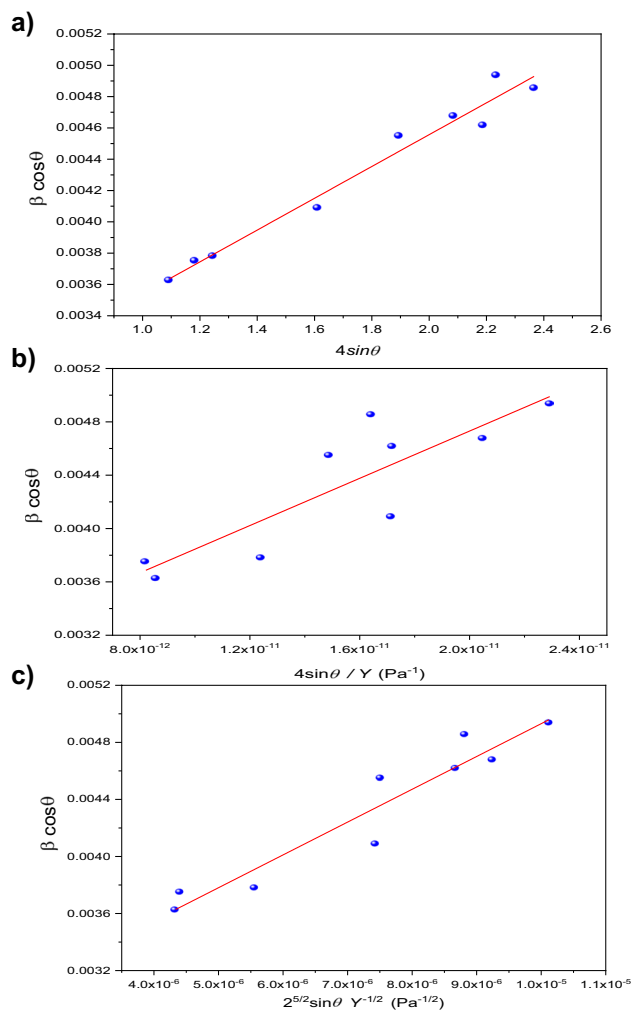
Fig. 2 The plots of **a)** $\beta\cos\theta$ vs. $4\sin\theta$, **b)** $\beta\cos\theta$ vs. $4\sin\theta/Y$, and **c)** $\beta\cos\theta$ vs. $2^{5/2}\sin\theta\, Y^{-1/2}$

$$L = \sqrt{\frac{a^2}{3} + c^2 \left(0.25 - \frac{a^2}{3c^2}\right)^2} \qquad (9)$$

$$APF\% = \frac{2\pi a}{3\sqrt{3}c} \times 100 \qquad (10)$$

The L value was estimated to be 1.9783 Å. For the hexagonal crystal structure, the APF% value is 74%. For the as-prepared ZnO sample, this value was found to be 75.46%.

The truncated hexagonal pyramid morphology is seen in the SEM images of the ZnO sample shown in Fig. 3. The average size of the experimental nanocluster has been determined as 5.598 μm, which was calculated by Imagej Software using the SEM image. The EDX result supports the formation of the ZnO structure.

Geometry

After the optimization of the constrained $[ZnO]_{25}(H_2O)_4$ and $[ZnO)_{55}(H_2O)_4$ clusters, their c-axis lengths were calculated as 13.1 Å and 29.2 Å, respectively (Figs. 4 and 5). As a result of the calculations, the Zn-O bond length of the optimized $[ZnO]_{55}(H_2O)_4$ cluster was calculated as 1.93 Å at the Zn-terminated (0001) surface and 1.90 Å

at the O-terminated (000) surface. Considering that the bond length in bulk ZnO in the wurtzite structure is 1.96 Å, it is seen that there is a shortening of 1.5% in the Zn-terminated surface and 3.1% in the O- terminated surface. The bond length at the core of the nano-particle was found to be slightly higher than the experimental value of bulk ZnO. The Zn-O bond length in the interior of the nanoparticle was calculated as 1.99 Å, which is 1.5% longer than the experimental value. We have experimentally calculated this value as 1.9783 Å mentioned in the experimental section. Similarly, the O-Zn-O bond angle was calculated as 112.2° at the Zn-terminated surface and 118.8° at the O-terminated surface. Compared to this angle of 109.2 in bulk ZnO, the O-Zn-O angle increased by 2.7% and 8.8% in Zn- and O-terminated surfaces, respectively. The O-Zn-O angles in the inner part of the cluster were calculated as 104.7° and were found to be 4.5% smaller than the experimentally measured value.

Similarly, when geometrical parameters such as bond angle and bond length of $[ZnO]_{25}(H_2O)_4$ cluster were analyzed, it was observed that these parameters were similar to $[ZnO]_{55}(H_2O)_4$ cluster and there was no significant difference. When the geometrical parameters obtained as a result of the calculations are compared with bulk ZnO, it is seen that the values are in agreement with each other
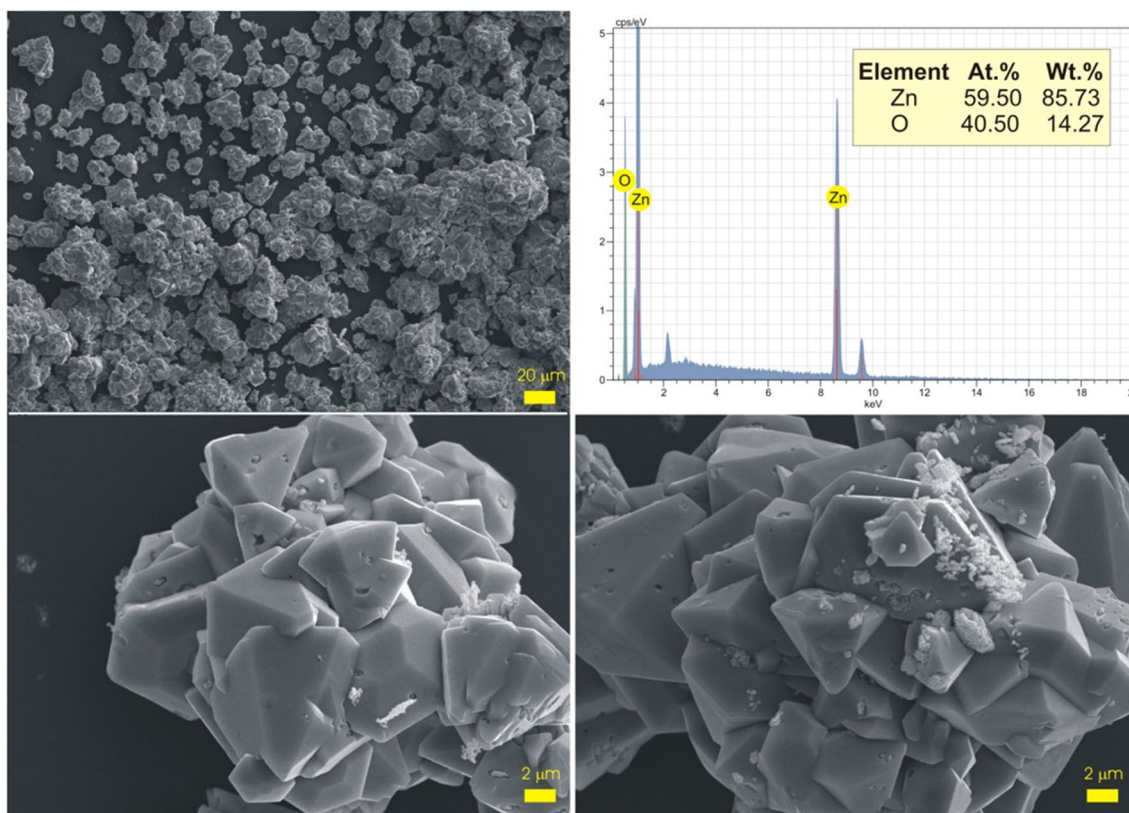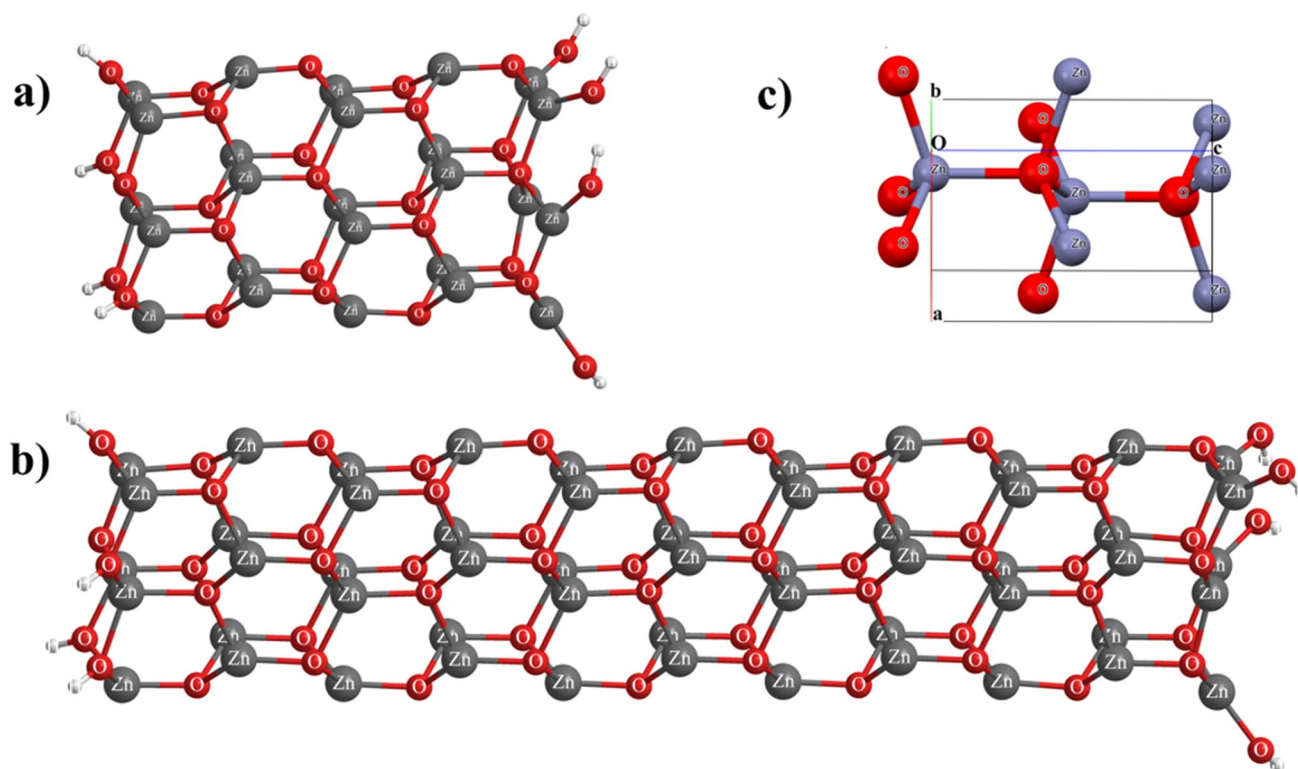

Fig. 3 SEM images and EDX report of ZnO

Fig. 4 Optimized geometrical structures of the (**a**) $[(ZnO)_{25}(H_2O)_4]$, (**b**) $(ZnO)_{55}(H_2O)_4$ 2D nanostructures. (**c**) Crystal structure of wurtzite ZnO
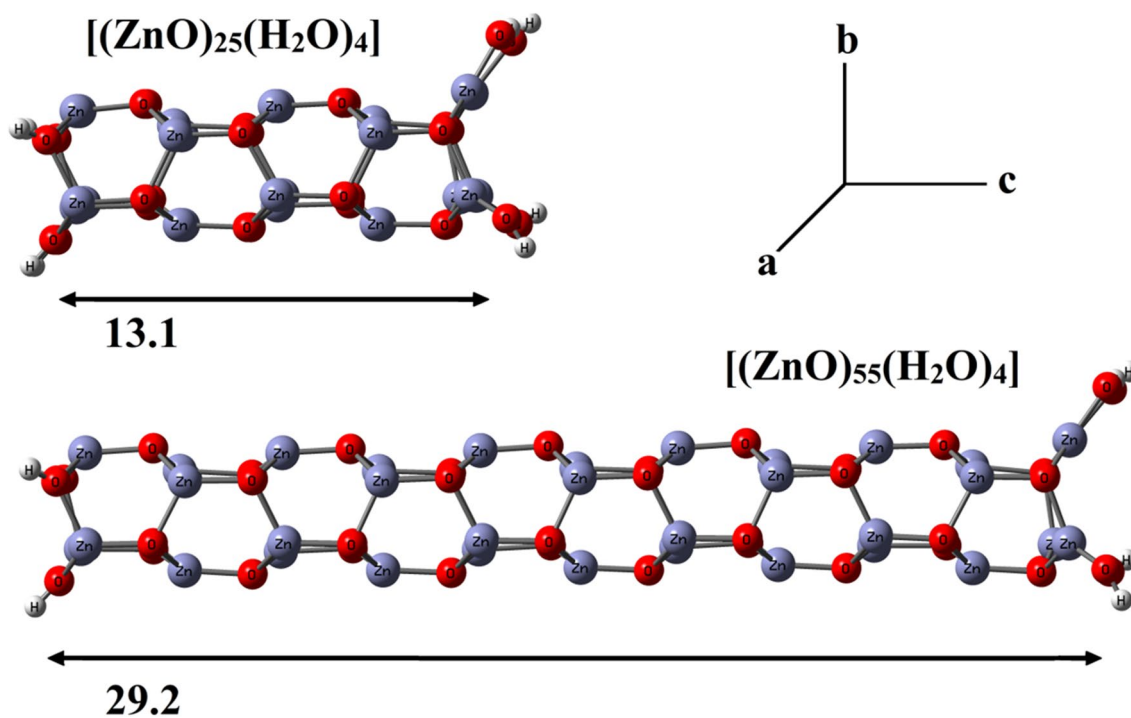

Fig. 5 Optimized geometrical structures, seen along the c crystallographic axis. The wire lengths (Å) are also reported

and there is no phase transition from wurtzite to rock salt during the optimization process.

Electronic structure and absorption spectra

In the energy calculations of $[ZnO]_{55}(H_2O)_4$ cluster in vacuum, the HOMO energy level of this structure is -6.03 eV, LUMO energy level is -3.04 eV and HOMO-LUMO band gap is 2.99 eV. Similarly, the energy calculations of the $[ZnO]_{25}(H_2O)_4$ cluster showed that the HOMO energy level was -6.68 eV, the LUMO energy level was -2.47 eV and the HOMO-LUMO band gap was 4.27 eV. As the length in the c direction decreases, the band gap increases due to quantum confinement effects. In the present study, the variation of the band gap with respect to the c direction is in parallel with the previously reported studies [46, 51]. However, it should be noted that the variation of the band gap with respect to the c direction does not differ much after a certain length (about 5 nm) [46, 51]. It is observed that the HOMOs and LUMOs calculated in both clusters are distributed throughout the system rather than on polar surfaces (Fig. 6). As can be seen from this distribution, the saturation of the polar surfaces with dissociating water molecules prevented the formation of surface localized trap states of atoms lacking coordination.

A more precise prediction of the excitation energies of confined nanostructures needs TD-DFT computations,

despite the fact that Kohn-Sham (KS) molecular orbitals and their eigenvalues can provide a fair estimate for the bandgap of bulk II-VI semiconductor materials. TD-DFT calculations more accurately predict bandgap transitions by taking into
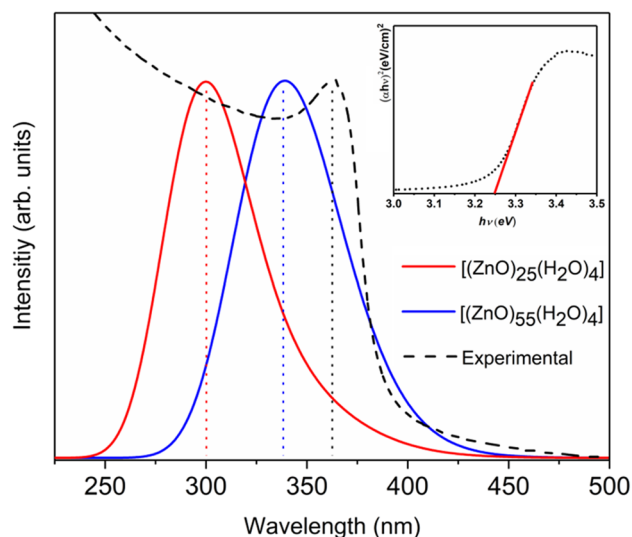

Fig. 7 Experimental and calculated absorption spectra of the ZnO nanostructures, obtained by a Gaussian convolution with FWHM = 0.333 eV, calculated taking into account the 16 lowest singlet−singlet electronic transitions. The inset show the Tauc plot of the optical transmittance spectra of the ZnO nanoparticles

Fig. 6 Isodensity plots of the frontier orbitals of the $[(ZnO)_{25}(H_2O)_4]$ cluster
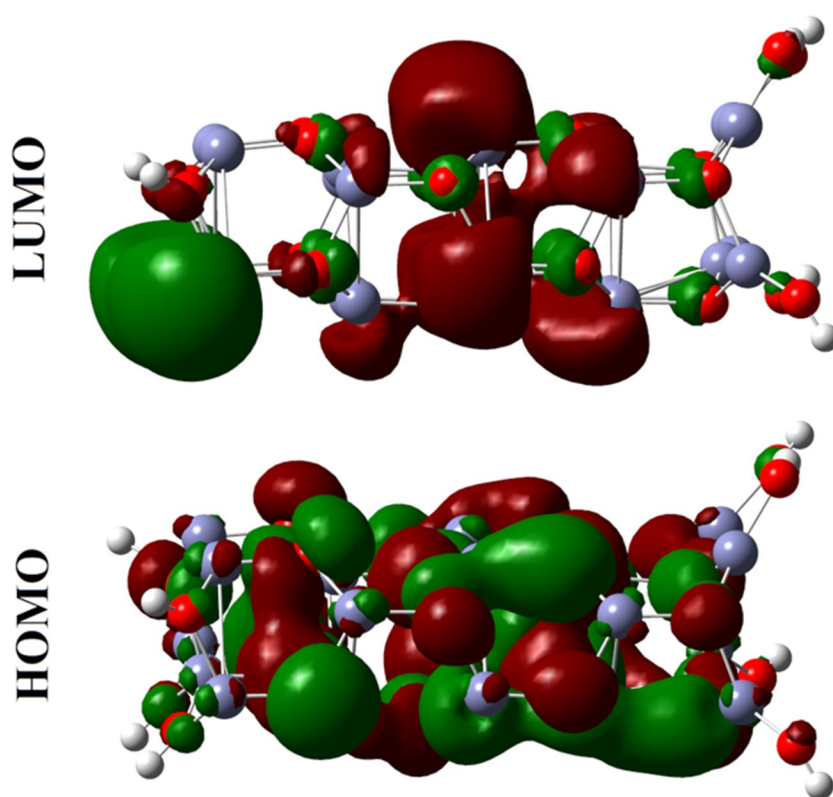
account electron-hole interactions, exchange-correlation effects, and configurational mixing of single excitations. Figure 7 shows the TD-DFT spectra of $[ZnO]_{55}(H_2O)_4$ and $[ZnO]_{25}(H_2O)_4$ clusters for the 16 lowest electronic transitions. According to these spectra, the calculated lowest excitation energies are 3.13 eV (396 nm) for $[ZnO]_{55}(H_2O)_4$ and 3.61 eV for $[ZnO]_{25}(H_2O)_4$. Considering that the experimental value determined by the Tauch plot in Fig. 7 is 3.25 eV, it is seen that the TD-DFT calculated band gap transitions for $[ZnO]_{55}(H_2O)_4$ cluster are quite compatible with the experimental value.

To better comprehend the electronic structures of the nanoparticles, density of states (DOS) and partial density of states (PDOS) plots of $[ZnO]_{25}(H_2O)_4$ and $[ZnO]_{55}(H_2O)_4$ clusters were plotted as shown in Fig. 8. The PDOS analysis of the nanocluster is very important in terms of providing information about the contribution of atomic orbitals to the CB (conduction band) and VB (valence band). As can be seen from Fig. 8a and b, the VB edge is significantly affected

by the change in the size of the clusters. On the other hand, there is no significant difference in the variation of CB edge energy with cluster size. However, it was found that the band gap decreases with the increase in the number of atoms in the clusters. As can be seen in previously reported studies [36, 50, 51, 61, 62], the systematic decrease in band gap with the increasing number of atoms in clusters is attributed to the quantum confinement effect in nanoclusters. The identification of the observed peaks may be done easily because the valence band structures of all the binary tetrahedrally coordinated semiconductors are comparable. Accordingly, following the notation suggested in the literature [63], the valence band features are labeled as P_I, P_{II} and d. The peak labeled as P_I originates from the 2p orbitals of the O atom and is clearly visible in Fig. 8d, which shows the partial density of states analysis for the $[ZnO]_{55}(H_2O)_4$ cluster.

Similarly, the P_{II} and d peaks are associated with the 4s and 3d orbitals of the Zn atom, respectively, and this relationship is shown in Fig. 8d. The 4s and 4p orbitals of the Zn atom make
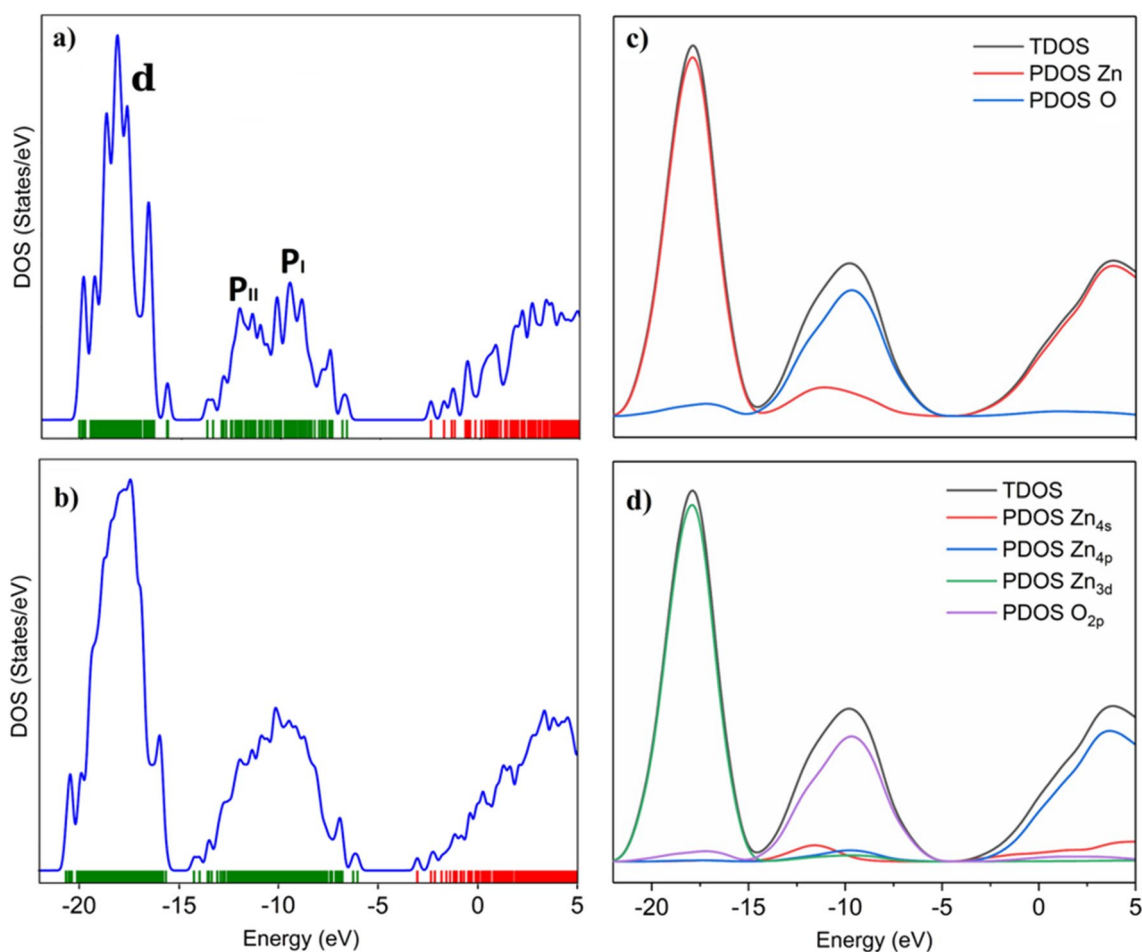

Fig. 8 DOS of (**a**) $[(ZnO)_{25}(H_2O)_4]$ and (**b**) $ZnO)_{55}(H_2O)_4]$ obtained by a Gaussian convolution of fwhm = 0.50 eV of the individual KS orbitals (green = occupied and red = virtual orbitals). Partial density of states (PDOS) (**c-d**) of $[(ZnO)_{55}(H_2O)_4]$ cluster, obtained by a Gaussian convolution of fwhm = 1.03 eV

up the majority of the low-lying empty orbitals in the conduction band. The relationship of the P$_I$, P$_{III}$ and d peaks with the orbitals in the present study was found to be in great agreement with the experimental and theoretical studies in the literature [50, 51].

If the PDOS graphs are interpreted on an atom basis (Fig. 8c), it is seen that the Zn atom makes the highest contribution to the d peak and conduction band peak, while the O atom makes the highest contribution to the P$_I$ peak. When the DOS plots of $[ZnO]_{25}(H_2O)_4$ and $[ZnO]_{55}(H_2O)_4$ clusters are analyzed (Fig. 8a and b), it is seen that with the increase in the number of atoms in the clusters, a broadening occurs in the P$_I$, P$_I$ and d peaks.

Conclusions

In this study, calculation of the structural, electronic and optical properties of $[ZnO]_{25}(H_2O)_4$ and $[ZnO]_{55}(H_2O)_4$ clusters has been carried out and the obtained results have been compared with both experimental data and available data in literature. In order to create a realistic ZnO nanoparticle model, the lowest optical transition energies of $[ZnO]_{25}(H_2O)_4$ and $[ZnO]_{55}(H_2O)_4$ clusters were calculated by DFT/TD-DFT methods. The simulations showed that the $[(ZnO)_{55}(H_2O)_4]$ cluster was a good model for attaining the structural, optical, and electrical features discovered experimentally. In UV–VIS calculations, it was confirmed that the band gap decreases with the increase the number of atoms in cluster. On the other hand, the DOS calculations showed that the HOMO energy level increase with the increase the number of atoms in the clusters and no significant change was found in the LUMO energy levels. In addition, it was found that the CAM-B3LYP functional highly successful in reproducing the experimental data reported in the present study and previously reported data. Furthermore, the lowest excitation energy in TD-DFT calculations of the identical system is in perfect agreement with the experimental value with a difference of 0.1 eV.

Data availability The datasets generated during and/or analyzed during the current study are available from the corresponding author onreasonable request.

Declarations

Ethical approval Not applicable.

Competing interests The authors have no relevant financial or nonfinancial interests to disclose.

References

1. Wei S, Lian J, Chen X, Jiang Q (2008) Effects of seed layer on the structure and property of zinc oxide thin films electrochemically deposited on ITO-coated glass. Appl Surf Sci 254:6605–6610. https://doi.org/10.1016/j.apsusc.2008.04.039

2. Baviskar PK, Nikam PR, Gargote SS et al (2013) Controlled synthesis of ZnO nanostructures with assorted morphologies via simple solution chemistry. J Alloys Compd 551:233–242. https://doi.org/10.1016/j.jallcom.2012.10.052

3. Meng Y, Lin Y, Lin Y (2014) Electrodeposition for the synthesis of ZnO nanorods modified by surface attachment with ZnO nanoparticles and their dye-sensitized solar cell applications. Ceram Int 40:1693–1698. https://doi.org/10.1016/j.ceramint.2013.07.065

4. Hsu C-H, Chen D-H (2011) Photoresponse and stability improvement of ZnO nanorod array thin film as a single layer of photoelectrode for photoelectrochemical water splitting. Int J Hydrogen Energy 36:15538–15547. https://doi.org/10.1016/j.ijhydene.2011.09.046

5. Bai S, Sun C, Guo T et al (2013) Low temperature electrochemical deposition of nanoporous ZnO thin films as novel NO2 sensors. Electrochim Acta 90:530–534. https://doi.org/10.1016/j.electacta.2012.12.060

6. Przeździecka E, Gościński K, Stachowicz M et al (2013) Spectrum selective UV detectors from an p-ZnO:As/n-GaN diodes grown by Molecular Beam Epitaxy. Sensors Actuators A Phys 195:27–31. https://doi.org/10.1016/j.sna.2013.02.021

7. Guo H, Zhou J, Lin Z (2008) ZnO nanorod light-emitting diodes fabricated by electrochemical approaches. Electrochem Commun 10:146–150. https://doi.org/10.1016/j.elecom.2007.11.010

8. Sharma SK, Rammohan A, Sharma A (2010) Templated one step electrodeposition of high aspect ratio n-type ZnO nanowire arrays. J Colloid Interface Sci 344:1–9. https://doi.org/10.1016/j.jcis.2009.12.026

9. Hsieh C-T, Yang S-Y, Lin J-Y (2010) Electrochemical deposition and superhydrophobic behavior of ZnO nanorod arrays. Thin Solid Films 518:4884–4889. https://doi.org/10.1016/j.tsf.2010.03.081

10. Cao B, Cai W, Li Y et al (2005) Ultraviolet-light-emitting ZnO nanosheets prepared by a chemical bath deposition method. Nanotechnology 16:1734–1738. https://doi.org/10.1088/0957-4484/16/9/054

11. Liang Y-C (2012) Growth and physical properties of three-dimensional flower-like zinc oxide microcrystals. Ceram Int 38:1697–1702. https://doi.org/10.1016/j.ceramint.2011.08.028

12. Abd-Ellah M, Moghimi N, Zhang L et al (2013) Effect of electrolyte conductivity on controlled electrochemical synthesis of zinc oxide nanotubes and nanorods. J Phys Chem C 117:6794–6799. https://doi.org/10.1021/jp312321t

13. Lin C, Lin H, Li J, Li X (2008) Electrodeposition preparation of ZnO nanobelt array films and application to dye-sensitized solar cells. J Alloys Compd 462:175–180. https://doi.org/10.1016/j.jallcom.2007.07.104

14. Ding Y, Wang ZL (2007) Profile imaging of reconstructed polar and non-polar surfaces of ZnO. Surf Sci 601:425–433. https://doi.org/10.1016/j.susc.2006.07.063

15. Özgür Ü, Alivov YI, Liu C et al (2005) A comprehensive review of ZnO materials and devices. J Appl Phys 98:041301. https://doi.org/10.1063/1.1992666

16. Wang ZL (2004) Zinc oxide nanostructures: growth, properties and applications. J Phys Condens Matter 16:R829–R858. https://doi.org/10.1088/0953-8984/16/25/R01

17. Hahn Y-B (2011) Zinc oxide nanostructures and their applications. Korean J Chem Eng 28:1797–1813. https://doi.org/10.1007/s11814-011-0213-3

18. Pál E, Hornok V, Oszkó A, Dékány I (2009) Hydrothermal synthesis of prism-like and flower-like ZnO and indium-doped ZnO structures. Colloids Surf A Physicochem Eng Asp 340:1–9. https://doi.org/10.1016/j.colsurfa.2009.01.020

19. Umavathi S, AlSalhi MS, Devanesan S et al (2020) Synthesis and characterization of ZnO and Ca-ZnO nanoparticles for potential antibacterial activity and plant micronutrients. Surf Interfaces 21:100796. https://doi.org/10.1016/j.surfin.2020.100796

20. Giannoudakos A, Agelakopoulou T, Asteriadis I et al (2008) Development and characterization of ZnO, Au/ZnO and Pd/ZnO thin films through their adsorptive and catalytic properties. J Chromatogr A 1187:216–225. https://doi.org/10.1016/j.chroma.2008.01.082

21. El Mragui A, Daou I, Zegaoui O (2019) Influence of the preparation method and ZnO/(ZnO + TiO2) weight ratio on the physicochemical and photocatalytic properties of ZnO-TiO2 nanomaterials. Catal Today 321–322:41–51. https://doi.org/10.1016/j.cattod.2018.01.016

22. Li F, Bi W, Liu L et al (2009) Preparation and characterization of ZnO nanospindles and ZnO@ZnS core–shell microspindles. Colloids Surf A Physicochem Eng Asp 334:160–164. https://doi.org/10.1016/j.colsurfa.2008.10.016

23. Fujinami A, Ogata S, Shibutani Y, Yamamoto K (2006) Adsorption process of Zn_2O_2 on a crystal polyimide surface. Model Simul Mater Sci Eng 14:S95–S103. https://doi.org/10.1088/0965-0393/14/5/S11

24. Kaygili O, Ercan I, Ates T et al (2018) An experimental and theoretical investigation of the structure of synthesized ZnO powder. Chem Phys 513:273–279. https://doi.org/10.1016/j.chemphys.2018.08.021

25. Arul Hency Sheela J, Lakshmanan S, Manikandan A, Arul Antony S (2018) Structural, Morphological and Optical Properties of ZnO, ZnO:Ni2+ and ZnO:Co2+ Nanostructures by Hydrothermal Process and Their Photocatalytic Activity. J Inorg Organomet Polym Mater 28:2388–2398. https://doi.org/10.1007/s10904-018-0909-5

26. Asture A, Rawat V, Srivastava C, Vaya D (2022) Investigation of properties and applications of ZnO polymer nanocomposites. Polym Bull. https://doi.org/10.1007/s00289-022-04243-w

27. Baranov AN, Sokolov PS, Solozhenko VL (2022) ZnO under pressure: from nanoparticles to single crystals. Crystals 12:744. https://doi.org/10.3390/cryst12050744

28. Raha S, Ahmaruzzaman M (2022) ZnO nanostructured materials and their potential applications: progress, challenges and perspectives. Nanoscale Adv 4:1868–1925. https://doi.org/10.1039/D1NA00880C

29. Chu L, Xu C, Zeng W et al (2022) Fabrication and application of different nanostructured ZnO in ultraviolet photodetectors: a review. IEEE Sens J 22:7451–7462. https://doi.org/10.1109/JSEN.2022.3158650

30. Puspasari V, Ridhova A, Hermawan A et al (2022) ZnO-based antimicrobial coatings for biomedical applications. Bioprocess Biosyst Eng. https://doi.org/10.1007/s00449-022-02733-9

31. Yadav SK, Sadowski T, Ramprasad R (2010) Density functional theory study of ZnX (X = O, S, Se, Te) under uniaxial strain. Phys Rev B 81:144120. https://doi.org/10.1103/PhysRevB.81.144120

32. Ren D, Xiang B, Gao Y et al (2017) Ab initio study of lattice instabilities of zinc chalcogenides ZnX (X=O, S, Se, Te) induced by ultrafast intense laser irradiation. AIP Adv 7:095021. https://doi.org/10.1063/1.4999445

33. Saha S, Pal S, Sarkar P et al (2012) A complete set of self-consistent charge density-functional tight-binding parametrization of zinc chalcogenides (ZnX; X=O, S, Se, and Te). J Comput Chem. https://doi.org/10.1002/jcc.22945

34. Saha S, Sarkar S, Pal S, Sarkar P (2013) Ligand mediated tuning of the electronic energy levels of ZnO nanoparticles. RSC Adv 3:532–539. https://doi.org/10.1039/C2RA22429A

35. Kohan AF, Ceder G, Morgan D, Van de Walle CG (2000) First-principles study of native point defects in ZnO. Phys Rev B 61:15019–15027. https://doi.org/10.1103/PhysRevB.61.15019

36. Lany S, Zunger A (2005) Anion vacancies as a source of persistent photoconductivity in II-VI and chalcopyrite semiconductors. Phys Rev B 72:035215. https://doi.org/10.1103/PhysRevB.72.035215

37. Janotti A, Van de Walle CG (2007) Native point defects in ZnO. Phys Rev B 76:165202. https://doi.org/10.1103/PhysRevB.76.165202

38. Shen X, Allen PB, Muckerman JT et al (2007) Wire versus tube: stability of small one-dimensional ZnO nanostructures. Nano Lett 7:2267–2271. https://doi.org/10.1021/nl070788k

39. Yanai T, Tew DP, Handy NC (2004) A new hybrid exchange-correlation functional using the Coulomb-attenuating method (CAM-B3LYP). Chem Phys Lett 393:51–57. https://doi.org/10.1016/j.cplett.2004.06.011

40. Jacquemin D, Le BT, Adamo C, Ciofini I (2012) What is the "best" atomic charge model to describe through-space charge-transfer excitations? Phys Chem Chem Phys 14:5383. https://doi.org/10.1039/c2cp40261k

41. Charaf-Eddin A, Planchat A, Mennucci B et al (2013) Choosing a functional for computing absorption and fluorescence band shapes with TD-DFT. J Chem Theory Comput 9:2749–2760. https://doi.org/10.1021/ct4000795

42. Ciofini I, Le Bahers T, Adamo C et al (2012) Through-space charge transfer in rod-like molecules: lessons from theory. J Phys Chem C 116:11946–11955. https://doi.org/10.1021/jp3030667

43. Monticone S, Tufeu R, Kanaev AV (1998) Complex nature of the UV and visible fluorescence of colloidal ZnO nanoparticles. J Phys Chem B 102:2854–2862. https://doi.org/10.1021/jp973425p

44. van Dijken A, Meulenkamp EA, Vanmaekelbergh D, Meijerink A (2000) Identification of the transition responsible for the visible emission in ZnO using quantum size effects. J Lumin 90:123–128. https://doi.org/10.1016/S0022-2313(99)00599-2

45. Kahn ML, Cardinal T, Bousquet B et al (2006) Optical properties of zinc oxide nanoparticles and nanorods synthesized using an organometallic method. ChemPhysChem 7:2392–2397. https://doi.org/10.1002/cphc.200600184

46. De Angelis F, Armelao L (2011) Optical properties of ZnO nanostructures: a hybrid DFT/TDDFT investigation. Phys Chem Chem Phys 13:467–475. https://doi.org/10.1039/C0CP01234C

47. Meyer B (2004) First-principles study of the polar O-terminated ZnO surface in thermodynamic equilibrium with oxygen and hydrogen. Phys Rev B 69:045416. https://doi.org/10.1103/PhysRevB.69.045416

48. Li C, Guo W, Kong Y, Gao H (2007) First-principles study on ZnO nanoclusters with hexagonal prism structures. Appl Phys Lett 90:223102. https://doi.org/10.1063/1.2743934

49. Wander A, Harrison NM (2001) The stability of polar oxide surfaces: The interaction of H2O with ZnO(0001) and ZnO(0001̄). J Chem Phys 115:2312–2316. https://doi.org/10.1063/1.1384030

50. Azpiroz JM, Mosconi E, De AF (2011) Modeling ZnS and ZnO nanostructures: structural, electronic, and optical properties. J Phys Chem C 115:25219–25226. https://doi.org/10.1021/jp2083709

51. Azpiroz JM, Infante I, Lopez X et al (2012) A first-principles study of II–VI (II = Zn; VI = O, S, Se, Te) semiconductor nanostructures. J Mater Chem 22:21453. https://doi.org/10.1039/c2jm33744d

52. Frisch MJ, Trucks GW, Schlegel HB et al (2009) Gaussian 09, Revision B.01. Gaussian 09, Revis. B.01, Gaussian, Inc., Wallingford CT

53. Hay PJ, Wadt WR (1985) Ab initio effective core potentials for molecular calculations. Potentials for K to Au including the outermost core orbitals. J Chem Phys 82:299–310. https://doi.org/10.1063/1.448975

54. Runge E, Gross EKU (1984) Density-functional theory for time-dependent systems. Phys Rev Lett 52:997–1000. https://doi.org/10.1103/PhysRevLett.52.997

55. Lu T, Chen F (2012) Multiwfn: a multifunctional wavefunction analyzer. J Comput Chem 33:580–592. https://doi.org/10.1002/jcc.22885

56 O'boyle NM, Tenderholt AL, Langner KM (2008) cclib: A library for package-independent computational chemistry algorithms. J Comput Chem 29:839–845. https://doi.org/10.1002/jcc.20823

57. Nielsen AB, Holder AJ (2009) Gauss view 5.0, user's reference. GAUSSIAN Inc, Pittsburgh

58. Okur HE, Bulut N, Ates T, Kaygili O (2019) Structural and optical characterization of Sm-doped ZnO nanoparticles. Bull Mater Sci 42:199. https://doi.org/10.1007/s12034-019-1877-2

59. Cullity BD (1978) Elements of X-ray diffraction, 2nd edn. Addison-Wesley Publ Co, Read, 100-105,277-279. https://doi.org/10.1119/1.1934486

60. Ibrahim EH, Albulym O, Kaygili O et al (2019) Green synthesis, structural, in vitro and in vivo bioactivity properties of ZnO nanoparticles for biomedical applications. J Biomater Tissue Eng 9:731–738. https://doi.org/10.1166/jbt.2019.2046

61. Reiss P, Protière M, Li L (2009) Core/shell semiconductor nanocrystals. Small 5:154–168. https://doi.org/10.1002/smll.200800841

62. Schrier J, Demchenko DO, Lin-Wang AAP (2007) Optical properties of ZnO/ZnS and ZnO/ZnTe heterostructures for photovoltaic applications. Nano Lett 7:2377–2382. https://doi.org/10.1021/nl071027k

63. Ley L, Pollak RA, McFeely FR et al (1974) Total valence-band densities of states of III-V and II-VI compounds from x-ray photoemission spectroscopy. Phys Rev B 9:600–621. https://doi.org/10.1103/PhysRevB.9.600